Rapid assessment of REBCO CC angular critical current density $J_c(B, T = 4.2\ \mathrm{K}, \theta)$ using torque magnetometry up to at least 30 tesla

To cite this article: J Jaroszynski *et al* 2022 *Supercond. Sci. Technol.* **35** 095009

OPEN ACCESS
IOP Publishing
Superconductor Science and Technology
Supercond. Sci. Technol. **35** (2022) 095009 (11pp)
https://doi.org/10.1088/1361-6668/ac8318

Rapid assessment of REBCO CC angular critical current density $J_c(B, T = 4.2\ \text{K}, \theta)$ using torque magnetometry up to at least 30 tesla

J Jaroszynski*, A-M Constantinescu, G Miller, A Xu, A Francis, T Murphy and D C Larbalestier

National High Magnetic Field Laboratory, Florida State University, 1800 E. Paul Dirac Drive, Tallahassee, FL, United States of America

E-mail: jaroszy@magnet.fsu.edu

Received 2 April 2022, revised 14 July 2022
Accepted for publication 21 July 2022
Published 2 August 2022

Abstract

Detailed design of $REBa_2Cu_3O_{7-x}$ (REBCO)-based magnets ideally relies on knowledge of the full angular and wide temperature range characterization of the critical current I_c of the REBCO coated conductors (CC) at high magnetic fields. In practice, however, obtaining $I_c(B, T, \theta)$ data by the commonly used electrical transport technique is expensive, tedious, and difficult, due to high critical current values that exceed 2000 A for $B||ab$-plane ($\theta = 90$ deg). The conductors are often damaged during angular transport measurements at angles approaching the *ab*-plane. Therefore, so far, REBCO magnets have been designed without full $I_c(B, T, \theta)$ data sets. Here, we present $J_c(B, T, \theta)$ results for more than twenty samples of CC all made to the same advanced pinning specification produced by SuperPower Inc. For this, we employed torque magnetometry, benchmarking the results to transport I_c measurements mostly made away from *ab*-plane, finding good agreement with scaling factors ≈1–1.3. What is striking is the huge variety of properties exhibited by the samples, even for CC made recently. Given the huge attention now being paid to the effects of screening currents and to the torques generated by offsets between the tape plane and the local magnetic field vector, our data set suggests some caution in detailed design of such magnets without having data of the type presented here.

Keywords: REBCO CC, angular critical current, magnet technology

(Some figures may appear in colour only in the online journal)

1. Introduction

$REBa_2Cu_3O_{7-x}$ (REBCO, where RE = rare earth elements) based coated (super)conductors (CC) are produced by several commercial manufacturers. Industrial manufacture has made possible all–superconducting 30 T—class magnets [1–4] with inner and outer coils made from REBCO and low temperature superconductors, respectively. Fairly recently, a small REBCO test coil ('little big coil'—LBC) produced a magnetic field $B = 14.4$ T inside a $B = 31.1$ T water cooled resistive magnet, pushing the world record of DC field to $B = 45.5$ T [5]. This test showed the feasibility of building REBCO magnets well beyond 30 T. Currently, several laboratories around the world are attempting to build superconducting magnets stronger than 30 T; some of them are EMFL (30 T/40 T)

* Author to whom any correspondence should be addressed.

[6], MIT (30.5 T) [7], Sendai (30 T) [8], RIKEN (32.5 T) [9], Hefei/Tsinghua (35 T) [10], and CAPP (30.5 T) [11]. Recently, the NHMFL has started a 40 T user magnet design project [12], building on the lessons learned from the 32 T all superconducting user magnet.

Unlike magnets made from isotropic conductors like Nb–Ti, Nb_3Sn or Bi-2212, magnets made from REBCO must deal with a very marked superconducting (and mechanical) anisotropy. Isotropic magnets generally have their performance limited by the region of maximum field, but magnets made from REBCO CC have a much more complex performance envelope. Solenoids now have their critical points not in the central windings but in the end windings where the radial fields depress the local critical current I_c far below that found for B parallel to the *ab*-planes at $\theta = 90$ deg.

The large angular variation of I_c forces the central windings to operate at currents far below the critical current, meaning that induced screening currents dominate the winding, generating significant body forces and error fields [13]. Large torques may also now be generated when the tape plane and local B vector diverge. For these and other reasons, systematic critical current (I_c) characterizations over a wide range of magnetic fields (B), temperatures, and angles (θ) are desirable. So far it is rare that they have been available. Close to the *ab*-planes, θ values can reach several kiloamperes at low temperatures, making the usual transport current methods of I_c measurement difficult to use. Indeed, this is why there are so few sets of $I_c(B,T,\theta)$ data available for $B \gtrsim 20$ T, $T \lesssim 30$ K, and $\theta \sim 90$ deg—where B is close to the *ab* plane.

The high I_c values of REBCO CC allow, conceptually, for design of magnets that could reach magnetic fields of 40 T and beyond. But as our 45.5 T Little Big Coil showed, damage is very often the consequence of operating in this very high field range. Based on this experience, we believe that it will be essential to carefully select the CC, above all based on a detailed understanding of the $I_c(B,\theta)$ characteristics of each tape used in the magnet due to the widely varying conditions of each winding in the magnet. For now, pancake winding is the most common method used for solenoid manufacture. At the ends of the solenoid, especially at its outer edges, there are regions subjected to strong radial components of the total field, where the field angle θ is far from 90 deg and I_c is low. In contrast $I_c(B,T,\theta \approx 90\,\text{deg})$ is several times larger in the center of the solenoid; this condition of the transport current I being much less than I_c negatively influences the magnet performance for at least three reasons. First, it is difficult to induce a normal state in central regions where I/I_c is small due to the huge I_c margin, making it very difficult to dissipate the stored magnetic energy throughout the whole magnet during a quench. This spatially inhomogeneous heat dissipation may be catastrophic for the magnet. Second, excessively high I_c values lead to huge screening currents which may cause mechanical damage due to excessive stress. Third, any conductor movement due to the large Lorentz forces or torques may induce additional screening currents and heating, leading to quench and potential degradation.

In principle, such a complex field, field-angle profile in the magnet might suggest a design philosophy for the conductor in which the conductor should display a tailored lengthwise $I_c(x)$ profile in which $I_c(x)$ increases smoothly from the inner towards the outer magnet turns so as to balance the sharp $I_c(B,T,\theta)$ dependence of REBCO itself. However, at this time, even the simplest $I_c(x)$ profile (i.e. $I_c(x) \approx$ const.) is not available, as some $I_c(x)$ fluctuations are always present [14]. Further, significant differences are often found between manufactured CC tapes with identical nominal specifications [15, 16]. However, such unintentional $I_c(x)$ variations, also allow for some intentional sorting of the conductor between end and central pancakes. Such considerations reinforce the need for a new, effective tool for tape characterization at low T, which would enable better conductor selection.

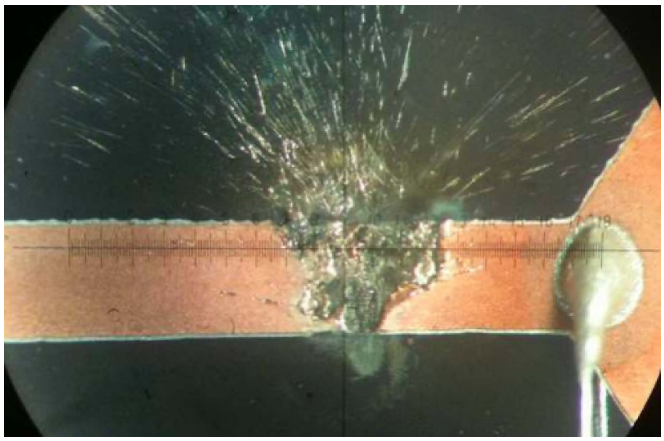

Figure 1. A photo of 0.9 mm wide ReBCO bridge burnt after current has reached 850 A for the $B||ab$-plane configuration in LHe. This advanced R&D sample was made at University of Houston and measured at the NHMFL [17]. One voltage tap is seen at right.

As mentioned before, conventional transport measurements are extremely difficult to perform at low temperatures where I_c is high and in strong fields where strong electromagnetic forces and torques develop. The main difficulty consists in delivering kiloamp currents to a rotating platform inside a very limited space. Indeed, when $B||ab$-plane, critical currents in 4 mm wide tape, may reach $I_c \gtrsim 2000$ A at 4.2 K. Further, current leads have so far been out of REBCO tapes to reduce heat dissipation; these are fragile and difficult to secure in the presence of very strong Lorentz forces, often breaking during measurements. Moreover, I_c dropouts can produce a substantial electric field E locally, due to the strong nonlinearity of the $E(I)$. The resulting voltages barely contribute to the overall voltage measured on the voltage taps, but they may generate local heating and sample damage (figure 1). Furthermore, screening currents induced during field sweeps and sample rotations add to the problem. These screening currents are comparable to transport critical currents, and exert significant forces and torques on both the sample and current leads. Indeed they exist even if no transport current is applied when the REBCO is inserted inside a powered external magnet.

Beside all of the above, accessibility to strong magnetic field in resistive magnets is limited and measurements are costly, requiring a high amount of energy. The early attempts [18–20] could not access high ($B \gtrsim 20$ T) fields, low

($T \lesssim 30$ K) temperatures, and angles $75° \lesssim \theta \lesssim 105°$ around the *ab*-plane. Thus only rather limited data sets are available for developers of high field magnets [21–31].

The angular I_c at elevated temperatures (around 77 K) has received much attention; this regime displays a rich vortex pinning phenomenology and a complicated angular current profile [32], reflecting a pinning landscape arising from multiple types of pinning centers. In contrast, the angular $I_c(\theta)$ range around $\theta = 90$ deg was seldom investigated at LHe temperatures; the first measurements reported [21, 23] revealed that the $I_c(\theta)$ profile is much simpler at $T = 4.2$ K than at elevated temperatures. Here, $I_c(\theta)$ shows a minimum (or very weak maximum for BZO doped samples) at $\theta = 0$ with a smooth variation up to a pronounced maximum at $\theta = 90$ deg. The full width at half maximum (FWHM) around the ab plane ($\theta = 90$ deg) is of order $\approx$12 deg at $B = 30$ T [24] for non-BZO samples and increases with higher densities of artificial pinning centers.

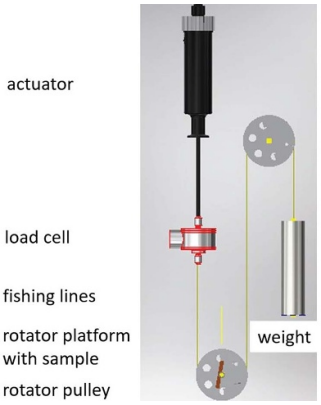

Figure 2. An idea of torque magnetometer used here. The actuator, driven by servo motor, rotates sample on the rotating platform with fishing lines. The load cell measures tension T of the line. The tension is proportional to the torque from the sample and the radius of rotator pulley plus balancing weight. $T = \tau \times r + W$.

2. The method

Instead of searching for solutions to mitigate the strong effects induced on CC samples by the significant torques arising from screening currents, we developed a device to measure the torque and assess $I_c(B,T,\theta)$ from torque values. This novel torque magnetometer (US patent pending) will be described elsewhere [33], while the idea is shown in figure 2. Indeed, it is well known that the magnetic moment $\vec{m}$ arising from induced screening currents is proportional to I_c up to a certain geometrical factor related to sample dimensions. Since, according to the magnetic moment definition, the torque is given by $\vec{\tau} = \vec{m} \times \vec{B}$, knowing the τ allows one to assess I_c. Moreover, it is widely accepted that the geometrical factor extracted from transport measurements at particular (B',T',θ') can be used to scale I_c from m made at any arbitrary (B,T,θ) [30].

In particular, for rectangular thin films like a REBCO CC a simple integration yields [34]:

$$m = \frac{1}{4} J_c t w^2 l \left(1 - \frac{w}{3l}\right) \tag{1}$$

where w, l, and t denote the sample width, length and thickness, respectively. The above formula was calculated assuming that J_c is homogenous, isotropic in plane, and that the sample plane is perpendicular to B.

However, when the sample is rotated vs. magnetic field around $\hat{\boldsymbol{x}}$ parallel to the longer side of the sample, the current flowing in the $\hat{\boldsymbol{y}}$-direction parallel to the shorter side, is not subjected to the full Lorentz force, as happens in the $\hat{\boldsymbol{x}}$-direction. This leads to $J_c^y > J_c^x$. The I^y current needs than a narrower path than I^x, leading to a redistribution of current, and equation (1) becomes:

$$m = \frac{1}{4} J_c t w^2 l \left(1 - \frac{w}{3l}\frac{J_c^x}{J_c^y}\right). \tag{2}$$

We do not know the exact J_c^x/J_c^y ratio, but clearly $J_c^x/J_c^y < 1$, which leads to an increase of the observed moment (and torque). Indeed, when the fraction of the sample that can accommodate the I^y current decreases, then a larger fraction can carry I^x which contributes to the torque around $\hat{\boldsymbol{x}}$. The data on J_c^y is scarce, but the J_c^y/J_c^x ratio can be substantial. In this case, the m and τ observed in a square sample ($w = l$) could be overestimated by roughly 50%. This error can be avoided only by employing long samples with high l/w aspect ratio, so that $w/3l \to 0$, as discussed in details in [35].

Our torque magnetometer can measure torque and, therefore, assess $J_c(B,T,\theta)$ over the full angular range 0°–360°. It can measure at temperatures ranging from LHe to $\lesssim$60 K, including the region just above 4.2 K, where transport measurements in He gas are virtually impossible because of high power and lack of effective cooling [36]. Importantly, it is compatible with both superconducting and resistive magnets at the NHMFL. Initial measurements were carried also in the 45 T hybrid magnet which has a smaller cold bore (only 16 mm vs. 39 mm in other magnets). This indicates that the magnetometer can be also scaled to e.g. popular physical property measuring systems. Further, the magnetometer accommodates large samples (usually 13 mm × 4 mm, 10 mm × 2 mm in the hybrid); in these samples the contributions of the reversible magnetization [37, 38] arising from vortices is negligible, the signal being dominated by induced macroscopic screening, or Bean [39] currents. If we reduce sample dimensions to use a cantilever torque magnetometer, the reversible magnetization will be a substantial part of the signal. This is because magnetic moment from screening currents scales as lw^2 while reversible magnetization just as the sample area lw. Also, for large l/w ratios the contribution of the return currents (parallel to $\hat{\boldsymbol{x}}$) at the sample's ends are practically eliminated [34, 35]. Further, measurements of full width samples can be used to study entangled electromagnetic and mechanical properties including high torques and stresses enhanced by screening current, which are both critical for magnet development. Again, the magnetic moment (and the torque) per sample area unit is proportional to sample width, as seen in equation (2). In addition, this torque magnetometer performs measurements very

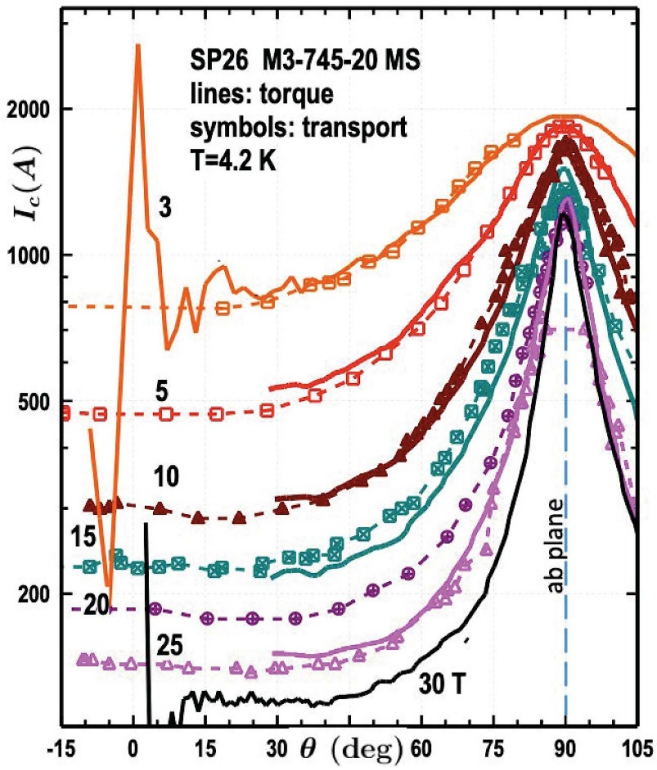

Figure 3. Comparison between transport and torque magnetometry data: $I_c(B,\theta)$ as a function of θ obtained by transport at $B = 3, 5, 10, 15, 20$, and 25 T (symbols and dashed lines) and data deduced from torque magnetometry at $B = 3, 5, 10, 15, 25$ and 30 T (solid line). These data were multiplied by $K = 1.1$ to fit transport data. Since the torque vanishes at $\theta = 0$, the calculated $I_c(\theta \to 0) \propto \tau(\theta)/\sin(\theta) \to 0/0$, is noisy around $\theta = 0$. However, at these angles I_c is low and it is easy to measure in transport.

fast, drastically reducing LHe consumption in comparison to traditional transport techniques. Lastly, the $I_c(B,T,\theta)$ values derived from torque measurements and multiplied by $K = 1.1$ are in good agreement with transport data, as demonstrated in figure 3. more general we found $K = 1$–1.3 comparing torque in other samples for which angular transport data are available [16, 24, 40].

3. Results and discussion

Many REBCO CC magnets today are designed with transport data on narrow bridges obtained by Xu *et al* [23, 24]. These data were later parameterized by Hilton *et al* [41] on a few 2010 vintage SuperPower advanced pinning tapes. In particular, sample M3-745-MS20 (or SP26 see #1 in table 1 and figure 3) became a widely used standard. It took 2 weeks of effort to obtain these far-from-perfect transport data. Many samples burnt or degraded during these measurements as shown in figure 1. Despite many attempts, there was no single point measured at 30 T while the 25 T data are also incomplete. Figure 3 compares these old transport angular I_c data together with the recent data obtained by torque. All the torque data are calculated from equation (1) and then multiplied by a factor of $K = 1.1$ to fit the transport data. It is clearly seen that there is a correspondence of these data sets with a maximum deviation of less than 20%. without any systematic deviations with B or θ. There are rather random differences connected to experimental statistical errors. The torque measurements took only an hour and a half. No sample degradation was observed, even at the highest field.

During measurement, the sample is rotated in field at a rate of 0.5 deg s^{-1} or less. However, weaker signals corresponding to configurations around the c-axis or at elevated temperatures take slightly longer. On the other hand samples that can carry high I_c values and/or are engineered with very thick REBCO layers require slower measurement, to avoid magneto-thermal instabilities. Nevertheless, measurements with our torque magnetometer can be performed fast, as it takes only about 3–6 min to measure over a range of angles θ such as, say, $-30 < \theta < 210$ deg. Effectively, we are able to measure torque in this angle range in 6–8 different magnetic fields in only one hour, which also includes the sample cool down. Thus, our method makes possible extensive testing in a fast and economical way. Indeed, we were able to characterize the angular critical current at different fields and temperatures in more than 50 samples at the highest fields available. Here we focus on the $I_c(B, 4.2\,\mathrm{K}, \theta)$ in LHe at various magnetic fields ranging from 5 to 30 T. The temperature dependence of samples with known nanostructural differences will be discussed in detail elsewhere [42].

Figure 4 shows results from three recent samples manufactured by SuperPower Inc. The samples are 'standard' marketed as advanced pinning centers (APC) product category with nominal Zr doping off 7.5%. However, their properties were graded by varying the REBCO thickness. It is clearly seen, that this process was quite successful.

Table 1 shows representative set of 25 samples manufactured between 2009–2020 and characterized by torque. Their superconducting film thickness varies by a factor of two, from 0.8 to 1.9 μm, while the copper stabilizer thickness ranges between 5 and 40 μm. The stoichiometry—that is, yttrium and gadolinium content—is also slightly different among samples, however we do not have any data from the vendor on this point. Samples were made in two different MOCVD reactors, M3 and M4. All the samples measured with torque used in this paper were marketed as advanced pinning centers (APC) product category with nominal Zr doping of 7.5%.

We can divide these samples into three groups:

(a) Older samples (#1–7) were grown between approx. 2009–2015
(b) Newer samples (#8–17) were grown in last 5 years, or so
(c) A set of 2020 samples #18–25 were cut from the same recent conductor. This allows us to see that small $I_c(77\,\mathrm{K})$ fluctuations translate into substantial (480–630 A at the *ab* plane).

Figures 5 and 7 illustrate how differently samples from older group A and newer B and C groups behave as a function of field and field angle. Figure 5 shows $I_c^{ab}(B)$ maxima at the *ab* plane plotted vs. field for several samples in semi-logarithmic scale. The I_c is normalized at $B = 5$ T for clarity.

Table 1. Parameters obtained from torque measurements. All the conductors used in the present study were delivered by SuperPower Inc. and made in MOCVD machines #M3 or #M4 to the same 'advanced pinning centers' (APC) formula with 7.5% BZO doping. The second and third columns show SuperPower and our labeling, respectively. The 4th column shows I_c at 30 T. The full width at half maximum (FWHM) at $B = 30$ T is shown in col. 5th. The FWHM was determined from experimental data as $\theta_R - \theta_L$, where $I_c(\theta_R) = I_c(\theta_L) = (I_c^{ab} + I_c^c)/2$. A fitting parameter ω from equation (7), listed in the next column, also describes the width of the I_c peak (it increases as peaks narrow, in contrast to FWHM). It also describes the anisotropy of the fitting function in equation (7). Parameter $\gamma_e = I_c^{ab}/I_c^c$ describes experimental anisotropy at $B = 30$ T. In turn column 8th shows experimental ratio of I_c^{ab} at 30 T and 5 T at the *ab* plane, while the last column shows a parameter describing exponential decay of I_c with field at the *ab* plane: $I_c^{ab} \propto \exp(-B/B_0)$ determined from fits.

#	SP name	Name	$I_c^{ab}(30\,\mathrm{T})$ (A)	FWHM (deg)	ω	$\gamma_e = \frac{I_c^{ab}(30\,\mathrm{T})}{I_c^{c}(30\,\mathrm{T})}$	$\frac{I_c^{ab}(30\,\mathrm{T})}{I_c^{ab}(5\,\mathrm{T})}$	B_0 (T)
1	M3-745-20	SP26	1240	10	17.7	10	0.67	66
2	M3-745-2	SP49	1051	9.6	18.5	8.2	0.76	96
3	M3-858	SP48	727	12.4	14.7	6.5	0.58	43
4	M4-218-2	SP139	1526	15.6	10	6.5	0.58	43
5	M3-1028-1	SP144	922	6.6	29	10.3	0.61	65
6	M4-245-3	SP180	1086	9.7	19	12	0.7	58
7	M4-253-2	SP215	1670	15.8	10.1	6.5	0.61	46
8	M4-576-3	D3	430	9.7	21	7	0.56	41
9	M4-576-4	D4	620	10.6	18	7.7	0.56	41
10	M3-1433-6	D5	676	14.3	12.8	5.8	0.54	38
11	M3-1433-6	D6	674	12.8	14.5	7.8	0.59	50
12	M3-1426-5	D7	1067	11.6	15.4	6.6	0.62	54
13	M3-1425-3	D8	1053	14	11.8	5	0.58	41
14	M3-1333-2	D9	584	11.8	17	8.1	0.54	37
15	M3-1352-3	H1	1210	16	11.2	6.1	0.62	40
16	M4-506-3	H2	864	14.4	11.1	5.8	0.53	38
17	M4-533-3	x-13	753	22	8.2	5.2	0.55	37
18	M4-526-6	a-1	621	19.4	9.2	5.1		
19	M4-526-6	c-3	623	17	10.2	5.1		41
20	M4-526-6	e-5	675	15.7	11.9	5.7	0.56	37
21	M4-526-6	f-6	540	21	8.3	4.5		
22	M4-526-6	g-7	493	21	8.6	4.7	0.45	29
23	M4-526-6	i-9	562	18	9.4	5.4	0.63	40
24	M4-526-6	k-11	495	21	8.5	4.6	0.47	30
25	M4-526-6	l-12	450	12.8	14.8	6.2	0.65	26

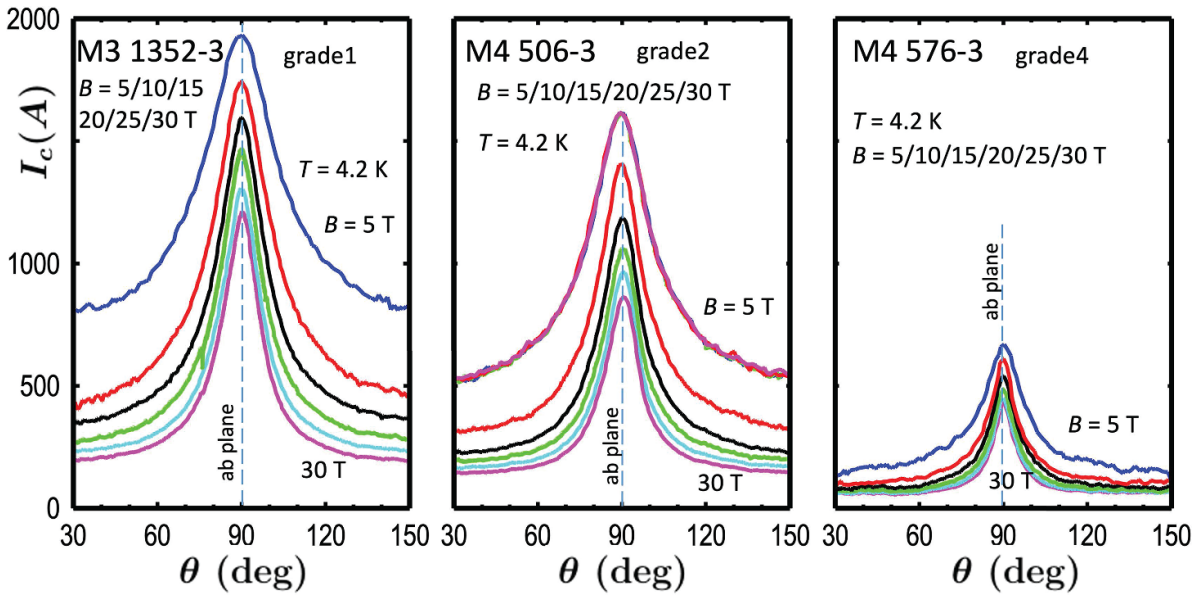

Figure 4. Critical current obtained from torque vs. angle measurements at various fields for three relatively new samples purchased for the NHMFL 40 T project. The conductors were intentionally graded to have different critical currents. As it is clearly seen, this procedure turns out to be quite successful.

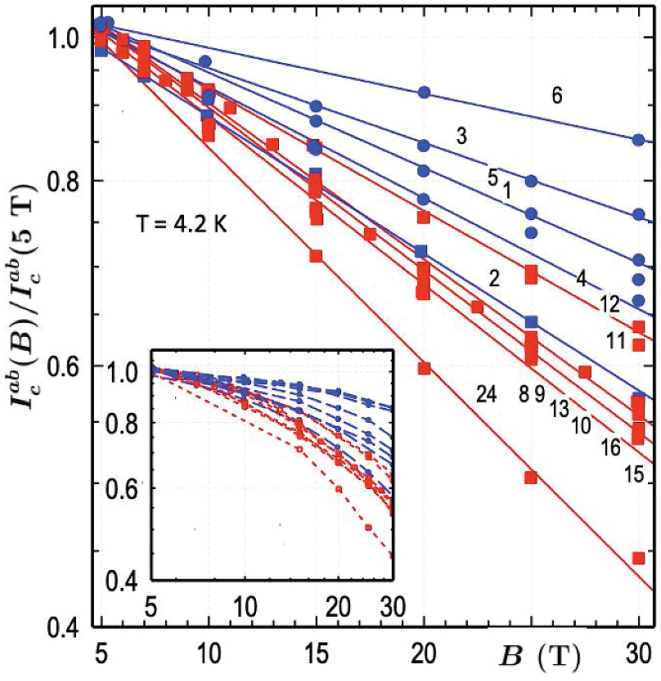

Figure 5. $I_c(\theta = 90\,\text{deg})$ for samples as a function of B plotted in semi-log scale. Data are normalized at $B = 5$ T, for clarity. Samples are labeled with numbers from table 1, however the most important point made here is that in the older samples (blue symbols) $I_c(B)$ decays slower than in the newer ones (red symbols). The solid lines represent exponential fits $I_c^{ab} \propto \exp(-B/B_0)$ (not all are shown). Fitting parameters B_0 are listed in table 1. The inset shows the same data plotted in log–log scale.

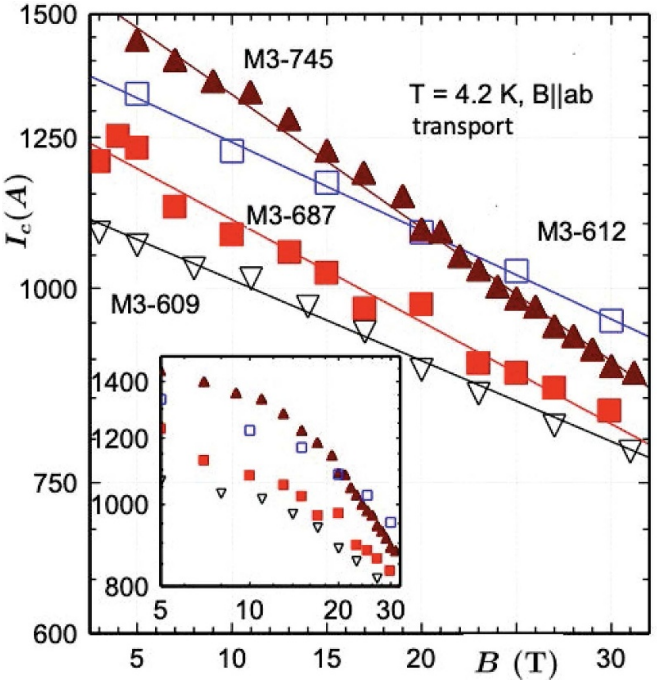

Figure 6. Transport data $I_c(\theta = 90\,\text{deg})$ vs. B for narrow ($w \approx 1$ mm) samples plotted in semi-log scale. The straight lines represent exponential fits $I_c^{ab} \propto \exp(-B/B_0)$. Samples M3-609, M3-612 are not doped, while M3-687 is nominally 10% BZO doped. These samples are not listed in table 1 as they were not measured by torque. Sample M3-745-20 is #1 in table 1, however it was cut from different part of the conductor. The parameter B_0 describing exponential decay was found to be 86, 78, 66, and 55 T, respectively. The inset show the same data plotted in log–log scale.

The inset shows the same data plotted in double logarithmic scale. Clearly, the data are much more linear in the semi-logarithmic scale, indicating that the data are better described by an exponential rather than a power function:

$$I_c^{ab}(B) = I_c^{B=0} \exp(-B/B_0). \tag{3}$$

In general, it is challenging to determine the functional dependence of $I_c(B)$ when this changes not more than 50% while B changes less than one order of magnitude (from 5 to 30 T). Figure 5 clearly shows that this dependence is closer to an exponential. This is in contrast to behavior observed away from the *ab* plane, where I_c is described by the power function $I_c(B) \propto B^{-\alpha}$, with $0.45 \lesssim \alpha \lesssim 1$ at 4.2 K. [24, 43] where α varies from $\alpha \approx 0.45$ for no-BZO samples to $\alpha \approx 1$ for strong BZO doping.

The exponential behavior observed here is also in contrast with theoretical predictions [44] and published scaling models [16, 30]. This discrepancy may stem from the different method of measurement employed. Further, we measured full width samples, where huge screening currents may give rise to large stress; this may cause, in turn, a faster $I_c^{ab}(B)$ decay. However, Branch *et al* [45, 46] has shown that elastic strains have only a small influence on I_c at $T = 4.2$ K, in contrast to elevated temperatures.

Figure 6 shows some old, partially published (but misinterpreted then) [24] transport data of $I_c^{ab}(B)$ which clearly show that $I_c^{ab}(B)$ decays exponentially for both BZO doped and not doped samples. This eliminates the method of measurement as the reason of the discrepancy between experiment and theoretical scaling models mentioned above. Well, the resistive data were taken on $w \lesssim 1$ mm bridges. According to equation (1), the induced current scales as w^2. Thus the current and the stress is ≈16 times lower than in the 4 mm wide samples used in torque measurements. Moreover, some of the resistive measurements were carried on samples cooled down at fixed angle $\theta \approx 90$ deg and without field, so screening currents were virtually zero. Hence, neither the stress nor the method contribute to the discrepancy between experimental data and theoretical models and assumptions.

Figure 7 shows the angular current deduced from the torque measurements at $B = 30$ T. All the samples are doped with 7.5% BZO. For clarity, traces are normalized to unity at $\theta = 90$ deg. As it is clearly seen, $I_c(\theta)$ decays with angle at significantly different rates for the various samples measured; this leads to a drastic variation of their anisotropy, $\gamma_e = I_c^{ab}/I_c^c$ reaching values as high as 10 for sample SP144 and only around 5 for samples #18–25, see table 1. The 'newer' samples display a lower anisotropy and wider *ab* peaks, characteristics which are beneficial for magnet applications. The sample SP26 made $\lesssim$2010, widely used for calculations and simulations, displays one of the sharpest *ab* peaks. Detailed TEM analysis [16, 27] has clearly shown that the observed variations of the

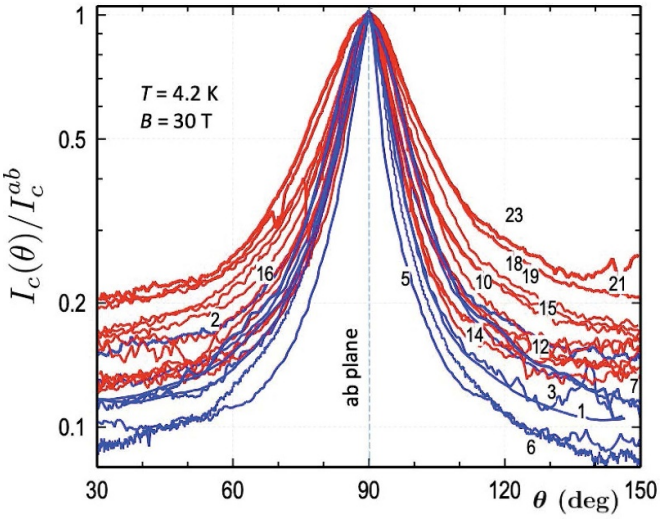

Figure 7. I_c vs. angle at $B = 30$ T for different samples. For clearer comparison, data are normalized to unity at $\theta = 90$ deg. Samples are labeled with the numbers from table 1, however the most important point here is that the newer samples (red lines) show wider $I_c(\theta)$ peaks around the *ab* plane than the older ones (blue lines).

anisotropy are strongly dependent on the quality of the BZO nanorod growth. In particular, they are affected by the density and length of the BZO columnar defects. Large pins do not determine pinning at low T, but their quality has a strong influence on the pinning via the strain that they introduce into the REBCO matrix and resulting potential fluctuations. In particular, the sample SP144 contains significantly poor quality BZO columns; consequently, it also displays the highest angular anisotropy and the sharpest *ab* peak. Moreover, it is also characterized by an anomalous angular critical current at 77 K although, normally, BZO doping leads to significantly higher I_c around the *c*-axis than at the *ab*-plane, as observed in samples SP26, 139, 180, 215. In SP144 these maxima are almost equal [16].

To sum up, 'older' conductors have sharper *ab* peaks but significantly weaker $I_c(B)$ field dependence. It is just the opposite in the 'newer' samples, which present wider *ab* peaks but faster $I_c^{ab}(B)$ decay. Whatever is the change in technology, it seems beneficial for magnet construction. Sharp angular anisotropy (I_c^{ab}/I_c^c reaching 10) limits magnet performance much more than I_c field dependence.

4. Parameterization

Several attempts were made to generate a functional description of the $I_c(B,\theta)$ data [28, 41, 47, 48]. The phenomenology at low T is much simpler than at high T. There is only one pronounced $I_c(\theta)$ peak at $T = 4.2$ K, located at the *ab* plane; in contrast, the $I_c(\theta)$ around the *c*-axis is quite flat [21, 23, 24, 27]. Theory, with some exceptions, does not deliver any analytical formula for $I_c(B,\theta)$. Indeed, this is a complicated many body phenomenon where the interactions between vortices and vortices with different landscapes of disorder must be taken into account. Moreover, in the region of strong magnetic field which is of interest here the density of vortices becomes very large. This leads to strong inter-vortex interactions and multi-vortex occupation of pinning centers. There are only rather qualitative assessments, such as [49] for weak interaction and low vortex densities. This model predicts a power function field dependence (with small logarithmic corrections) of the critical current, $I_c(B) \propto B^{-\alpha}$. The exponent is $\alpha \approx 0.5$, as observed, indeed, in non-BZO samples [24, 27] far from *ab* plane. In contrast, the so called anisotropic scaling approach [44] predicts for uncorrelated disorder that $I_c(B,\theta)$ scales merely with $B\epsilon$, where

$$\epsilon = \sqrt{\gamma^2 \cos^2(\theta) + \sin^2(\theta)}, \tag{4}$$

and $\gamma \approx 5$–7 is the electron mass anisotropy. This electronic mass anisotropy should not be confused with the experimental critical current anisotropy $\gamma_e = I_c^{ab}/I_c^c$ used in table 1. For clean samples, so called Ginzburg–Landau (G–L) scaling (equation (4)), sometimes works well at high temperatures [50]. It happens especially far from both the *ab* plane and the *c*-axis, where uncorrelated pinning dominates. Thus, some parametrization attempts use the magnetic field anisotropy factor $\epsilon(\theta)$ as a starting point to describe the angular I_c dependence. These practical approaches have just a formal, rather than physical, meaning. Using the large set of $I_c(B,\theta)$ data we collected, we compared the two formulae used previously [28, 41, 47].

The first formula contains the Ginzburg–Landau anisotropy term as defined in [28, 41] $\epsilon(\theta)$. Some models use $\epsilon(\theta)$ to some power κ, as in [27, 28, 51] and these are modified Kim's approaches.

$$I_c(B,\theta) = \frac{a(B) - c(B)}{\sqrt{\omega^2(B)\cos^2(\theta) + \sin^2(\theta)}} + c(B). \tag{5}$$

Sometimes the exponential approximations is used:

$$I_c(B,\theta) = \frac{a(B) - c(B)}{\exp(|\omega(B)(\theta - 90\,\mathrm{deg}|)} + c(B). \tag{6}$$

Here we introduce the 'cosine squared' formula:

$$I_c(B,\theta) = \frac{a(B) - c(B)}{\omega^2(B)\cos^2(\theta) + 1} + c(B), \tag{7}$$

where:

$$a(B) = a_1 \exp(-B/a_2),$$
$$c(B) = c_1 B^{-c_2},$$

and

$$\omega(B) = \omega_1 B^{\omega_2} \tag{8}$$

in equations (5)–(7).

Figure 8 clearly shows that all three fitting functions give resonable descriptions of the data around the *ab* peak. However, an exponential function is always too sharp around the *ab* plane, while G–L-like functions have long 'tails' and underestimate the I_c for angles closer to the *c*-axis. The 'cos square'

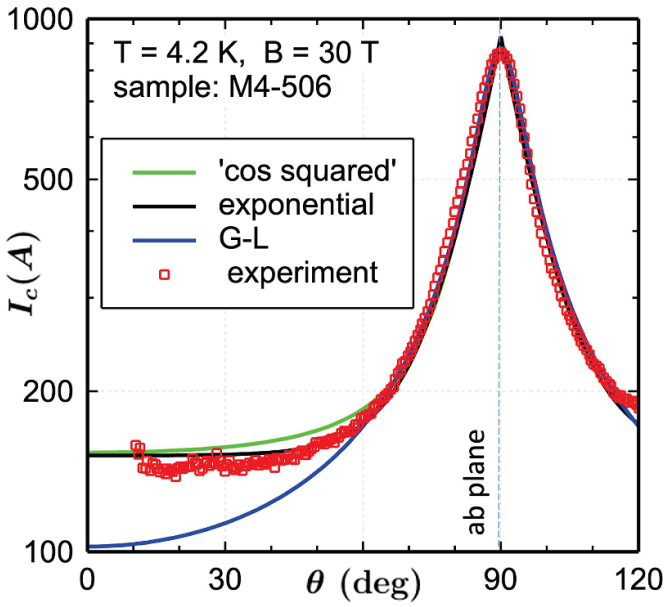

Figure 8. Comparison of fits made with equations (5)–(7).

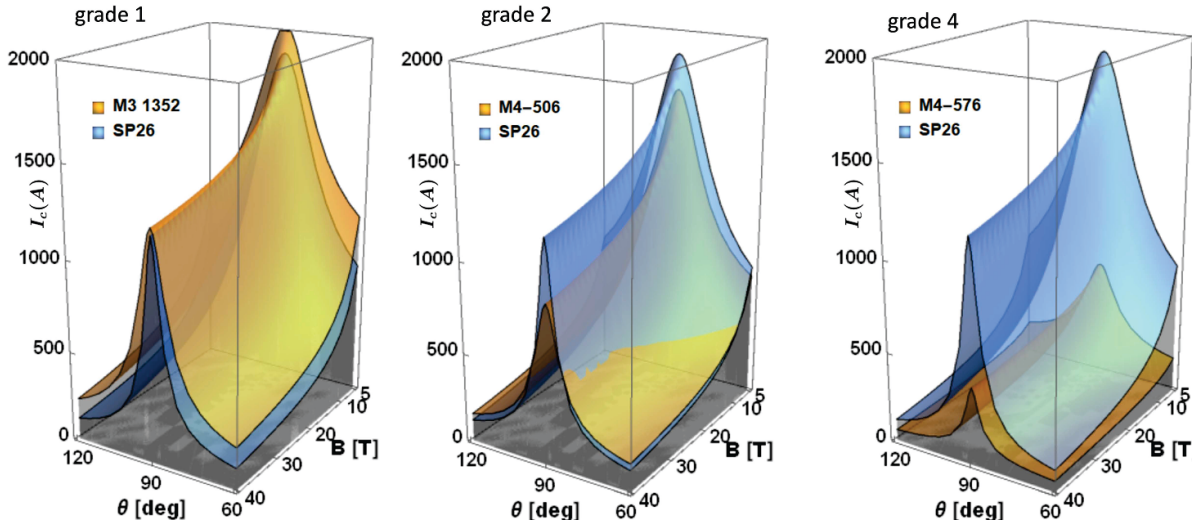

Figure 9. Critical current vs. field and angle for three different conductors (#15, #16, and #8 in table 1, also shown in figure 4). Values of of I_c were obtained from fits to experimental data using formula equation (7). For $5 \leqslant B \leqslant 30$ T the fitting procedure is an interpolation, while beyond 30 T it is an extrapolation.

function has the advantage of giving a good description both around the *ab* peak and closer to the *c*-axis. This is because I_c in equation (5). tends to $c(B)$ as $I_c \to 1/\cos(\theta) + c(B)$ for $\theta \to 0$, while for the 'cosine squared' expression equation (7). $I_c \to 1/\cos^2(\theta) + c(B)$, the first component vanishes much faster for small angles. Thus, I_c becomes just $I_c = c_1 B^{-c_2}$; this agrees very well with the observed $I_c \propto B^{-\alpha}$ in the range $0 < \theta \lesssim 45$ deg for BZO-doped samples [24, 27]. Equation (7) is somewhat connected to equation (5). but, again, without explicit physical meaning. The $\cos^2$ in the denominator simply describes better the $I_c(\theta)$ dependence near the *ab* plane (as the G–L model does too) and, at the same time the observed I_c flattening at angles closer to the *c*-axis (as an exponential function). As a result, good six parameter fits can be obtained without any starting values and constrictions. The Mathematica FindFit function was used in this global fit procedure in the angle-field space.

In previous attempts, the field dependences of the parameters ω and $a(B)$ were estimated with power functions or modified power functions. Here, because of the experimentally observed exponential field dependence $a(B) = a_1 \exp(-B/a_2)$, our parametrization describes the experimental data better in a wide range of angles and fields. In the range of $30 < \theta < 150$ deg, the fitting curves depart from the experimental data by 10% or less.

Figure 9 shows plots of $I_c(B, \theta)$ for three different 'new' samples used in the 40 T NHMFL project. These data are compared to the 'vintage' SP26 sample taken from the 32 T

NHMFL project. Surfaces were calculated from the fits in the $5 < B < 30$ T range and extrapolated beyond 30 T. Figure 9(b) clearly shows the non-trivial behavior of $I_c(B,\theta)$ for different (B,θ) ranges when the corresponding $I_c(B,\theta)$ surfaces interpenetrate. It is clearly seen, that 'newer' sample M4-505 (#16 in table 1), exhibits higher I_c at high fields and far from the *ab* plane than 'older' sample M3-745 (#1). This is very important region for magnet operation.

5. Summary

The rapid and inexpensive assessment of $I_c(B,T,\theta)$ delivers plenty of high field data that are very important for magnet design. It may also deliver data that may be important for materials science, where the full characterization of samples from different processes is essential for progress. Presented method also has the potential to explain the physics of pinning. So far, analytical—and even numerical—calculations describe poorly systems where there are more vortices than pinning sites, as it is at very high magnetic fields.

In particular, we determined parameters of dozens of tapes grown over the last decade with the same market specification, although not all are presented here. We found, that $I_c^{ab}(B)$ at the *ab* plane decays exponentially rather than with power function, as it was assumed so far. We also found some time-dependent changes in properties with recent production characterized by faster $I_c^{ab}(B)$ decay than in old samples. In turn, this is compensated by a slower $I_c(\theta)$ dependence. This weaker $I_c(\theta)$ anisotropy seems to be very beneficial for magnet construction. Intentional grading during the growth seems to work well, while unintentional lengthwise and conductor-to-conductor current fluctuations still exist.

From a long-term perspective, torque magnetometry can certainly help in the construction of more powerful scientific, nuclear fusion, NMR and accelerator magnets. Stronger, steady fields of all-superconducting magnets will also make it possible to explore various topics, such as high temperature superconductors under higher B/T ratios and new quantum states in 2D and 1D devices. There are many NHMFL users studying such structures who need measurements that require the highest possible fields for the longest possible time while tuning sample carrier density, shape and other properties using electric gates. Such measurements cost 10–20 times more if done in resistive magnets, compared to all-superconducting ones.

Data availability statement

The data that support the findings of this study are available upon reasonable request from the authors.

Acknowledgments

Many thanks to Bobby Joe Pullum who helped users at NHMFL DC Field Facility for almost thirty years. This work would not be possible without him.

The work was primarily funded by the National Science Foundation Cooperative Agreement No. DMR-1644779, the State of Florida, and by DMR-1644779 through User Collaborations Grants Program Project #5206. We acknowledge additional support by DOE-SC0022011 by the Office of Fusion Energy Sciences.

ORCID iD

J Jaroszynski https://orcid.org/0000-0003-3814-8468

References

[1] Cavallucci L, Breschi M, Ribani P L, Gavrilin A V, Weijers H W and Noyes P D 2019 A numerical study of quench in the NHMFL 32 T magnet *IEEE Trans. Appl. Supercond.* **29** 4701605
[2] Kolb-Bond D, Bird M, Dixon I R, Painter T, Lu J, Kim K L, Kim K M, Walsh R and Grilli F 2021 Screening current rotation effects: SCIF and strain in REBCO magnets *Supercond. Sci. Technol.* **34** 095004
[3] Liu J *et al* 2020 World record 32.35 tesla direct-current magnetic field generated with an all-superconducting magnet *Supercond. Sci. Technol.* **33** 03LT01
[4] Polenova T and Budinger T F 2016 Ultrahigh field NMR and MRI: science at a crossroads. Report on a jointly-funded NSF, NIH and DOE workshop, held on November 12–13, 2015 in Bethesda, Maryland, USA *J. Magn. Reson.* **266** 81
[5] Hahn S *et al* 2019 45.5-tesla direct-current magnetic field generated with a high-temperature superconducting magnet *Nature* **570** 496
[6] Song J-B, Chaud X, Debray F, Krämer S, Fazilleau P and Lécrevisse T 2022 Metal-as-insulation HTS insert for very-high-field magnet: a test report after repair *IEEE Trans. Appl. Supercond.* **32** 1–6
[7] Iwasa Y, Bascuñán J, Hahn S, Voccio J, Kim Y, Lécrevisse T, Song J and Kajikawa K 2015 A high-resolution 1.3-GHz/54-mm LTS/HTS NMR magnet *IEEE Trans. Appl. Supercond.* **25** 1–5
[8] Takahashi K, Okada T, Badel A, Awaji S, Miyazaki H, Hanai S and Ioka S 2021 Electromagnetic characteristics study of two-ply REBCO tapes pancake coils *IEEE Trans. Appl. Supercond.* **31** 1–5
[9] Yanagisawa Y, Hamada M, Hashi K and Maeda H 2022 Review of recent developments in ultra-high field (UHF) NMR magnets in the asia region *Supercond. Sci. Technol.* **35** 044006
[10] Zhang X, Liu H, Liu F, Shi Y, Qu T, Shao L, Hong Z and Guo L 2021 Progress in the construction of a 20 T REBCO insert coil for high-field all-superconducting magnets *IEEE Trans. Appl. Supercond.* **31** 1–4
[11] Gupta R, Anerella M, Ghosh A, Sampson W, Schmalzle J, Konikowska D, Semertzidis Y K and Shin Y 2016 High-field solenoid development for axion dark matter search at CAPP/IBS *IEEE Trans. Appl. Supercond.* **26** 1–5
[12] Bai H *et al* 2020 The 40 T superconducting magnet project at the national high magnetic field laboratory *IEEE Trans. Appl. Supercond.* **30** 1–5
[13] Xia J, Bai H, Yong H, Weijers H W, Painter T A and Bird M D 2019 Stress and strain analysis of a REBCO high field coil based on the distribution of shielding current *Supercond. Sci. Technol.* **32** 095005
[14] Hu X, Rossi L, Stangl A, Sinclair J W, Kametani F, Abraimov D, Polyanskii A, Coulter J Y, Jaroszynski J and Larbalestier D C 2017 An experimental and analytical study of periodic and aperiodic fluctuations in the critical current

of long coated conductors *IEEE Trans. Appl. Supercond.* **27** 9000205
[15] Rossi L, Hu X, Kametani F, Abraimov D, Polyanskii A, Jaroszynski J and Larbalestier D C 2016 Sample and length-dependent variability of 77 and 4.2 K properties in nominally identical RE123 coated conductors *Supercond. Sci. Technol.* **29** 054006
[16] Francis A, Abraimov D, Viouchkov Y, Su Y, Kametani F and Larbalestier D C 2020 Development of general expressions for the temperature and magnetic field dependence of the critical current density in coated conductors with variable properties *Supercond. Sci. Technol.* **33** 044011
[17] Xu A, Delgado L, Khatri N, Liu Y, Selvamanickam V, Abraimov D, Jaroszynski J, Kametani F and Larbalestier D C 2014 Strongly enhanced vortex pinning from 4 to 77 K in magnetic fields up to 31 T in 15 mol.% Zr-added (Gd, Y)-Ba-Cu-O superconducting tapes *APL Mater.* **2** 046111
[18] Kiss T *et al* 2002 Angular dependence of critical current properties in YBCO coated tape under high magnetic field up to 18 T *Physica* C **378–381** 1113–7
[19] Inoue M *et al* 2003 Estimation of *E–J* characteristics in a YBCO coated conductor at low temperature and very high magnetic field *Physica* C **392–396** 1078–82
[20] Inoue M *et al* 2007 Current transport properties of 200 A-200 m-class IBAD YBCO coated conductor over wide range of magnetic field and temperature *IEEE Trans. Appl. Supercond.* **17** 3207–10
[21] Uglietti D, Kitaguchi H, Choi S and Kiyoshi T 2009 Angular dependence of critical current in coated conductors at 4.2 K and magnet design *IEEE Trans. Appl. Supercond.* **19** 2909–12
[22] Otsuka A, Kiyoshi T and Takeda M 2010 A 1.3 GHz NMR magnet design under high hoop stress condition *IEEE Trans. Appl. Supercond.* **20** 596–9
[23] Xu A, Jaroszynski J J, Kametani F, Chen Z, Larbalestier D C, Viouchkov Y L, Chen Y, Xie Y and Selvamanickam V 2010 Angular dependence of J_c for YBCO coated conductors at low temperature and very high magnetic fields *Supercond. Sci. Technol.* **23** 014003
[24] Braccini V *et al* 2011 Properties of recent IBAD–MOCVD coated conductors relevant to their high field, low temperature magnet use *Supercond. Sci. Technol.* **24** 035001
[25] Inoue M, Fuger R, Higashikawa K, Kiss T, Awaji S, Namba M, Watanabe K, Iijima Y, Saitoh T and Izumi T 2011 In-field current transport properties of 600 A-class $GdBa_2Cu_3O_{7-\delta}$ coated conductor utilizing IBAD template *IEEE Trans. Appl. Supercond.* **21** 3206–9
[26] Molodyk A, Novozhilov M, Street S, Castellani L and Ignatiev A 2011 All-MOCVD technology for coated conductor fabrication *IEEE Trans. Appl. Supercond.* **21** 3175–8
[27] Xu A, Braccini V, Jaroszynski J, Xin Y and Larbalestier D C 2012 Role of weak uncorrelated pinning introduced by $BaZrO_3$ nanorods at low-temperature in (Y, Gd)$Ba_2Cu_3O_x$ thin films *Phys. Rev.* B **86** 115416
[28] Leys P M, Klaeser M, Schleissinger F and Schneider T 2013 Angle-dependent U(I) measurements of HTS coated conductors *IEEE Trans. Appl. Supercond.* **23** 8000604
[29] Benkel T, Miyoshi Y, Escamez G, Gonzales D, Chaud X, Badel A and Tixador P 2016 REBCO performance at high field with low incident angle and preliminary tests for a 10-T insert *IEEE Trans. Appl. Supercond.* **26** 4302705
[30] Senatore C, Barth C, Bonura M, Kulich M and Mondonico G 2016 Field and temperature scaling of the critical current density in commercial REBCO coated conductors *Supercond. Sci. Technol.* **29** 014002
[31] Tsuchiya K *et al* 2017 Critical current characterization of commercial REBCO coated conductors at 4.2 and 77 K *IEEE Trans. Appl. Supercond.* **27** 6600205
[32] Zhang Z, Zhou B, Liu J, Wang L and Wang Q 2022 Engineering-based design and fabrication procedure for mid-temperature REBCO magnets accommodating the strong I_c anisotropy *Superconductivity* **1** 100005
[33] Constantinescu A, Jaroszyński J, Miller G, and Larbalestier D C 2022 Novel torque magnetometer for high magnetic moments with strong anisotropy (US Patent pending; will be submitted to SUST)
[34] Gyorgy E M, Vandover R B, Jackson K A, Schneemeyer L F and Waszczak J V 1989 Anisotropic critical currents in $Ba_2YCu_3O_7$ analyzed using an extended Bean model *Appl. Phys. Lett.* **55** 283–5
[35] Thompson J R, Sinclair J W, Christen D K, Zhang Y, Zuev Y L, Cantoni C, Chen Y and Selvamanickam V 2009 Field, temperature and angle dependent critical current $J_c(H,T,\theta)$ in coated conductors obtained via contact-free methods *Supercond. Sci. Technol.* **23** 014002
[36] Goodrich L F, Cheggour N, Stauffer T C, Filla B J and Lu X F 2013 Kiloampere, variable-temperature, critical-current measurements of high-field superconductors *J. Res. Natl Inst. Stand. Technol.* **118** 301–52
[37] Fruchter L and Campbell I 1989 Torque in the irreversible regime on oriented $YBa_2Cu_3O_7$ crystals *Phys. Rev.* B **40** 5158–61
[38] Farrell D, Williams C, Wolf S, Bansal N and Kogan V 1988 Experimental-evidence for a transverse magnetization of the Abrikosov lattice in anisotropic superconductors *Phys. Rev. Lett.* **61** 2805–8
[39] Bean C 1964 Magnetization of high-field superconductors *Rev. Mod. Phys.* **36** 31
[40] Cheng J, Greenberg A, Jaroszynski J, Larbalestier D, Xu A, Lee J, Okada T, Awaji S, Senatore C and Sorbom B Parameterization of high temperature superconductor critical current data for various 2G HTS manufacturers (unpublished)
[41] Hilton D K, Gavrilin A V and Trociewitz U P 2015 Practical fit functions for transport critical current versus field magnitude and angle data from (RE)BCO coated conductors at fixed low temperatures and in high magnetic fields *Supercond. Sci. Technol.* **28** 074002
[42] Francis A, Jaroszynski J, Abraimov D, Kametani F and Larbalestier D Large range Jc(B,T,θ) study of commercial MOCVD REBCO Coated Conductors made to the same specification that show significant angular, field and temperature variations of vortex pinning
[43] Xu A *et al* 2017 J_e(4.2 K, 31.2 T) beyond 1 kA/mm^2 of a similar to 3.2 μm thick, 20 mol% Zr-added MOCVD REBCO coated conductor *Sci. Rep.* **7** 6853
[44] Blatter G, Feigelman M, Geshkenbein V, Larkin A and Vinokur V 1994 Vortices in high-temperature superconductors *Rev. Mod. Phys.* **66** 1125–388
[45] Branch P, Tsui Y, Osamura K and Hampshire D P 2019 Weakly-emergent strain-dependent properties of high field superconductors *Sci. Rep.* **9** 13998
[46] Branch P, Osamura K and Hampshire D 2020 Weak emergence in the angular dependence of the critical current density of the high temperature superconductor coated conductor REBCO *Supercond. Sci. Technol.* **33** 104006
[47] Long N J 2008 Model for the angular dependence of critical currents in technical superconductors *Supercond. Sci. Technol.* **21** 025007
[48] Talantsev E F and Mataira R C 2018 Polar projections for big data analysis in applied superconductivity *AIP Adv.* **8** 075213

[49] Ovchinnikov Y N and Ivlev B I 1991 Pinning in layered inhomogeneous superconductors *Phys. Rev.* B **43** 8024–9

[50] Civale L *et al* 2004 Understanding high critical currents in $YBa_2Cu_3O_7$ thin films and coated conductors *J. Low Temp. Phys.* **135** 87–98

[51] Chen Z, Kametani F, Chen Y, Xie Y, Selvamanickam V and Larbalestier D C 2009 A high critical current density MOCVD coated conductor with strong vortex pinning centers suitable for very high field use *Supercond. Sci. Technol.* **22** 055013